Characterization of Structural and Electronic Transitions During Reduction and Oxidation of Ru(acac)$_3$ Flow Battery Electrolytes by using X-ray Absorption Spectroscopy

Jonathan F. Kucharyson, Jason R. Gaudet, Brian M. Wyvratt, and Levi T. Thompson*[a]

Metal acetylacetonates possess several very attractive electrochemical properties; however, their cyclabilities fall short of targets for use in nonaqueous redox flow batteries. This paper describes structural and compositional changes during the reduction and oxidation of ruthenium(III) acetylacetonate [Ru(acac)$_3$], a representative acetylacetonate. Voltammetry, bulk electrolysis, and in situ X-ray absorption spectroscopy (XAS) results are complemented by those from density functional theory (DFT) calculations. The reduction of Ru(acac)$_3$ in acetonitrile is highly reversible, producing a couple at -1.1 V versus Ag/Ag$^+$. In situ XAS and DFT indicate the formation of [Ru(acac)$_3$]$^-$ with Ru–O bonds lengthened relative to Ru(acac)$_3$, nearly all of the charge localized on Ru, and no ligand shedding. The oxidation of Ru(acac)$_3$ is quasireversible, with a couple at 0.7 V. The initial product is likely [Ru(acac)$_3$]$^+$; however, this species is short-lived, converting to a product with a couple at -0.2 V, a structure that is nearly identical to that of Ru(acac)$_3$ within 3 Å of Ru, and approximately 70% of the charge extracted from Ru (balance from acetylacetone). This non-innocence likely contributes to the instability of [Ru(acac)$_3$]$^+$. Taken together, the results suggest that the stabilities and cyclabilities of acetylacetonates are determined by the degree of charge transfer to/from the metal.

1. Introduction

One of the major hurdles facing the integration of electricity derived from renewable resources into the grid is their temporal variability.[1] As a result, significant emphasis has been placed on the development of large-scale energy-storage devices. In addition to allowing the controlled distribution of renewable energy,[2] large-scale energy storage could enable higher efficiencies for existing energy generation technologies.[3]

Although a number of energy-storage technologies are being investigated,[4] redox flow batteries (RFBs) have been demonstrated to have a unique combination of attractive characteristics including long lifetimes, owing to their decoupled power and energy, and the potential to reach high energy densities.[5] RFBs consist of solvated active species (electrolytes) that are stored in reservoirs to prevent self-discharge.[5] These electrolytes are pumped past electrodes that are separated by a membrane. During charging, one of the electrolytes (catholyte) is oxidized and the other (anolyte) is reduced. The reverse occurs during discharge. For the purposes of clarity in this paper, the catholyte (oxidation) reaction will be referred to as the positive couple, and the anolyte (reduction) reaction will be referred to as the negative couple. All commercially available RFBs are based on aqueous electrolytes and, although they have been demonstrated to have long cycle lives,[5] the

electrochemical window of water (1.23 V)[6] results in relatively low energy densities and high cost. Darling et al. have indicated that an active species of sufficiently low molecular weight and high cell potential could enable nonaqueous RFBs that meet the aggressive Department of Energy goal of $100 per kWh.[7] Many nonaqueous solvents including acetonitrile allow for much higher potentials than water, in some cases as high as 5 V.[6]

A variety of metallo-organic[8–28] and organic complexes[29–33] have been investigated for use as active species in non-aqueous RFB electrolytes. Metal acetylacetonates such as V(acac)$_3$ and Cr(acac)$_3$ are particularly attractive, as they are capable of multielectron transfers, in some cases with redox couples that are separated by more than 2 V,[20,22,24] and their solubilities can be manipulated over more than four orders of magnitude through functionalization of the acetylacetone backbone.[26] Cycling solutions of metal acetylacetonates in acetonitrile reveals significant capacity fade that is often attributed to irreversible ligand shedding and/or irreversible oxidation reactions.[17–19,21,26] Chromium(III) bipyridine complexes have six redox couples over a 2 V window and solubilities approaching 1 M.[10] The multielectron transfer capabilities have been linked to non-innocence (redox activity) of the bipyridine ligands. When cycled in an H-cell, however, solutions of Cr(bpy)$_3$ in acetonitrile reach less than 30% of their theoretical capacities, and significant capacity fade occurs.[10] Wei et al. were able to cycle a ferrocenium complex [Fe(C$_5$H$_5$)$_2$CH$_2$N(CH$_3$)$_2$CH$_2$CH$_3$] N(SO$_2$CF$_3$)$_2$ in a flow cell for 100 cycles with 95% capacity retention at 0.1 M. When cycled at 0.8 M concentrations, however, significant capacity fade oc-

[a] J. F. Kucharyson, J. R. Gaudet, B. M. Wyvratt, Prof. L. T. Thompson
University of Michigan, Phoenix Memorial Lab
2301 Bonisteel Blvd, Ann Arbor, MI 48109 (USA)
E-mail: ltt@umich.edu

curred during the first 20 cycles.[34] The same group recently reported reduced capacity fade for the same complex at 1.2 m for 500 cycles in a static cell.[16] The cause of the fade, in most cases, has not been investigated and consequently is not well understood. Although cyclic voltammetry (CV) of these metallo-organic and organic complexes often demonstrates promising fundamental attributes, none possess sufficient cycle lives, in particular at the high concentrations needed for commercial applications.

Research described in this paper uses in situ X-ray absorption spectroscopy (XAS) to investigate the cause of instabilities for metal acetylacetonate-based electrolytes. XAS is one of the more powerful techniques for characterizing the electronic and physical structures of materials under in situ conditions. This technique utilizes high-energy X-rays that can be tuned to excite core electrons of a selected element. The resulting spectra consist of two regions: the X-ray absorption near-edge structure (XANES), which can be used to quantify the oxidation state of the element being investigated, and the extended X-ray absorption fine structure (EXAFS), which can be used to determine structural details. Apblett et al. recently reported the use of XAS to monitor the oxidation state and structural changes of an Fe-based ionic liquid (Fe[(OHCH$_2$CH$_2$)$_2$NH]$_6$-(CF$_3$SO$_3$)$_3$).[35] Partial charging was observed, but the exact oxidation state changes were not determined because of mixing issues within the cell. They also reported that the Fe—O bonds were lengthened during oxidation, as expected based on the anionic oxygens, but no bond lengths changes were detected during reduction. It is possible that side reactions occurred, as the electrolyte and cell were prepared while in contact with air.[35] To the best of our knowledge, this is the only report of the use of XAS to characterize a nonaqueous RFB electrolyte.

Although the cost and limited solubility of ruthenium(III) acetylacetonate [Ru(acac)$_3$] prevent it from being utilized as a commercial RFB active material, it does represent an interesting case study for understanding how the structures and charge distributions are affected by electrochemical oxidation and reduction. Owing to the weak X-ray absorption of acetonitrile at the Ru K edge (22 keV), transmission measurements through a functioning cell can probe the Ru without excessive signal loss through matrix absorption. Ru(acac)$_3$ was also selected because its properties are similar to those of the other metal acetylacetonates, and the cause for fade is unknown. Chakbarati et al. reported that, although Ru(acac)$_3$ undergoes two quasireversible redox reactions over a 2 V window in acetonitrile, less than 12% state of charge (SOC) was achieved during charge/discharge experiments.[27] This suggests that products formed during CV were different from those formed during charge/discharge experiments, or that the initial products converted to other species. In situ XAS will allow us to characterize these species. XAS was performed in specially designed electrochemical cells that allowed us to track changes in the structural and electronic properties of solvated Ru(acac)$_3$ while the material was being electrochemically oxidized or reduced, and isolated from air.

Our experimental protocol started by using CV to determine the voltage ranges to be used during oxidation and reduction

of the Ru(acac)$_3$ electrolytes. We then used bulk electrolysis (BE) to change oxidation states of the electrolytes. During BE, the electrolyte was held at a constant potential until a given degree of oxidation or reduction (i.e. SOC) was achieved, or until the current decayed to essentially zero. When possible, the BE was carried out in steps of 0.2 electrons per molecule. The resulting materials were characterized by using CV and XAS. In attempts to completely reduce Ru(acac)$_3$, the electrolyte was held at −1.5 V; subsequently, it was held at −0.7 V to fully reoxidize the electrolyte. In attempts to completely oxidize Ru(acac)$_3$, the electrolyte was held at 0.8 V; subsequently, it was held at 0.4 V to reduce the electrolyte. In situ XAS was performed in an air-tight Teflon-lined BE cell with windows to allow the X-ray beam to travel through the electrolyte. The experimental results were complemented by DFT structure optimization calculations using Gaussian 09, with Multiwfn for orbital density quantification.[36, 37] Together, the results allowed us to define the structural and compositional properties of the electrolyte and determine the cause for degradation of the Ru(acac)$_3$-based electrolytes.

2. Results and Discussion

2.1. CV and Standard Potentials

The cyclic voltammogram of Ru(acac)$_3$ in acetonitrile is illustrated in Figure 1. Voltammograms of Ru(acac)$_3$ solutions have been previously reported to include two quasireversible couples separated by approximately 1.77 V[27] and, as seen in
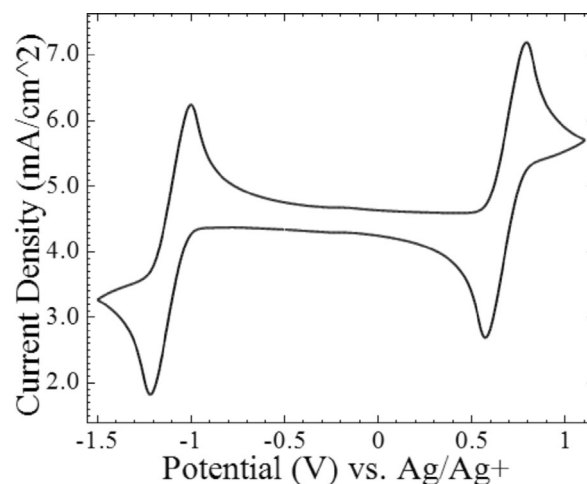

Figure 1. Cyclic voltammogram of 0.01 m Ru(acac)$_3$ in acetonitrile with 0.1 m TBABF$_4$.

Table 1, we observed similar results. Furthermore, the standard potentials generated by the DFT calculations were consistent with the experimental results. Figure 1 also reveals a minor couple at −0.2 V versus Ag/Ag$^+$ that was not previously reported. The origin of this feature will be discussed later.

The diffusion coefficient for Ru(acac)$_3$ in acetonitrile was determined by using the Randles–Sevcik equation,[20, 22, 24, 26] and

Table 1. Standard potentials (E_0) and diffusion coefficients (D_0) determined through CV and DFT calculations. The standard potentials in V versus Ag/Ag$^+$.

	E_0, negative couple [V]		E_0, positive couple [V]		D_0 [10^6 cm^2 s^{-1}]
	CV	DFT	CV	DFT	CV
Ru(acac)$_3$	−1.11	−1.09 ± 0.02	0.68	0.73 ± 0.09	6.1 ± 0.8

the results are listed in Table 1 (see Figures S1–S3 for scan-rate plots). This diffusion coefficient was within error of that for other acetylacetonate complexes,[26] which is not unexpected given their structural similarities. Although CV provides useful information regarding the short-term products of redox reactions, BE allows for the characterization of longer-term species that are more relevant to battery operation.

2.2. Structural Changes During Reduction and Oxidization

During BE, to completely reduce the Ru(acac)$_3$ solution, 0.95 electrons per molecule could be charged to the cell before the current decayed to zero, and 0.89 electrons per molecule could be extracted during the subsequent oxidation (see Figure S4). The small difference in the number of electrons is primarily attributed to cross-over, as voltammograms before and after BE were similar (Figure 2). Based on the literature,[27] the reaction associated with the couple at −1.1 V is [Eq. (1)]:
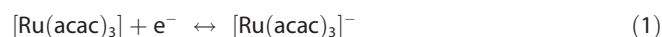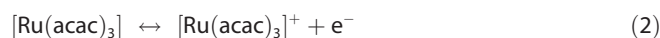
$$[Ru(acac)_3] + e^- \leftrightarrow [Ru(acac)_3]^- \qquad (1)$$

The results suggest that [Ru(acac)$_3$]$^-$ is not subject to further changes with time (i.e. it has a long shelf life). Also note that the couple at −0.2 V remains a very minor feature in the voltammogram and is inactive at the potentials used for BE.

During BE, to completely oxidize the Ru(acac)$_3$ solution, 1.11 electrons per molecule could be extracted from the cell before the current decayed to zero, but only 0.08 electrons per molecule could be charged to the cell during the subsequent
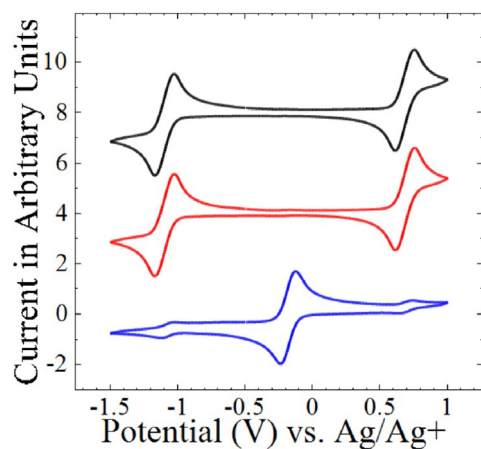
Figure 2. Cyclic voltammograms of Ru(acac)$_3$ electrolyte before (black), after reduction then oxidation (−1.5 V then −0.7 V) (red) and oxidation then reduction (0.8 V then 0.4 V) (blue).

reduction. The resting potential shifted from 0.7 to −0.2 V. In fact, the dominant couple in the CV after BE (Figure 2) is at −0.2 V; consequently, BE at 0.4 and 0.7 V would have little effect on the electrolyte. The principal reaction associated with the couple at 0.7 V has been reported to be [Eq. (2)]:[27]
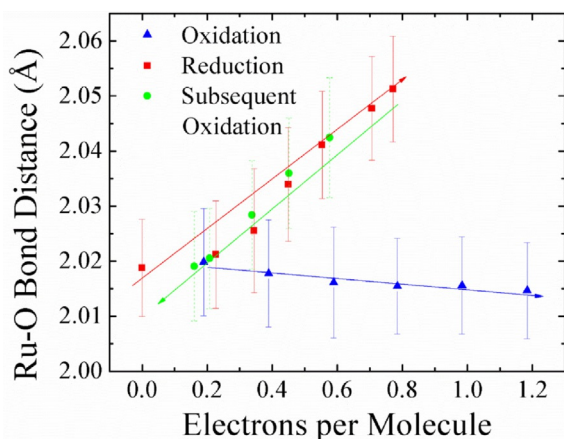
$$[Ru(acac)_3] \leftrightarrow [Ru(acac)_3]^+ + e^- \qquad (2)$$

Although the short-term product could be [Ru(acac)$_3$]$^+$ based on CV, results from BE suggest a different long-term product that yields a redox couple at −0.2 V. This product is not the free ligand, as the oxidation of acetylacetone is irreversible, occurring at approximately 0 V versus Ag/Ag$^+$.[38] The peak height of the product suggests a diffusion coefficient that is comparable to that for Ru(acac)$_3$ in acetonitrile and, based on the Stokes–Einstein equation,[39] this species is similar in size to Ru(acac)$_3$. The reversibility of the species giving rise to the couple at −0.2 V was characterized by reducing the electrolyte at −0.5 V, and subsequently oxidizing it at 0.4 V. The BE of this species was very irreversible. The emergence of this species would explain the difficulties reported previously in attempts to completely discharge cells employing Ru(acac)$_3$.[27]

EXAFS spectra of the electrolytes before and after BE are shown in Figure 3, along with illustrations of the relevant photoelectron paths. Each peak represents a half-path: the distance a photoelectron travels from the Ru atom to one or more scattering electrons and then back to the same Ru atom, divided by two according to convention. For single-scatterer paths, this is simply the distance from the Ru atom to the scattering atom; whereas, for two-scatterer paths, this is half the perimeter of the triangle formed by the scatterers and Ru. The peak at 1.6 Å corresponds to the approximate 2 Å path of a photoelectron to the six-fold oxygen nearest neighbor (R1). The peak at 2.5 Å corresponds primarily to the path of a photoelectron to the approximate 3 Å path of the six-fold carbon second-nearest-neighbor (R2), overlaid with the triangular half-path from the Ru around these same O and C atoms (R3, where the perimeter of this Ru—O—C triangle is 2R3). By using the Demeter software package, these three paths were generated from a DFT-optimized Ru(acac)$_3$ and fit to the experimental data. Before BE, the Ru—O bond distance (R1), the second-nearest-neighbor Ru—C distance (R2), and the Ru—O—C triangle (2R3) were found to be 2.02 ± 0.01 Å, 2.94 ± 0.02 Å, and 6.2 ± 0.1 Å, respectively (see Table S3). These distances indicate an O—Ru—C angle of 14°. The amplitude of this fit [where 1 represents Ru(acac)$_3$ and 0 represents a Ru atom with no local structure] was 1.0 ± 0.1 and the variance of these bond distances was found to be $\sigma^2 = 0.003 \pm 0.001$ Å, which is the expected value at room temperature; these values held during the entire course of the experiments.

The electrochemical reduction of Ru(acac)$_3$ causes the Ru—O bond (R1) to lengthen from 2.02 to 2.05 Å; subsequent oxidation causes the bond length to retract to its initial value (Figure 4). The average bond length varied linearly with the charge added or extracted per molecule. Although we expect these distances to represent two unique species—Ru(acac)$_3$
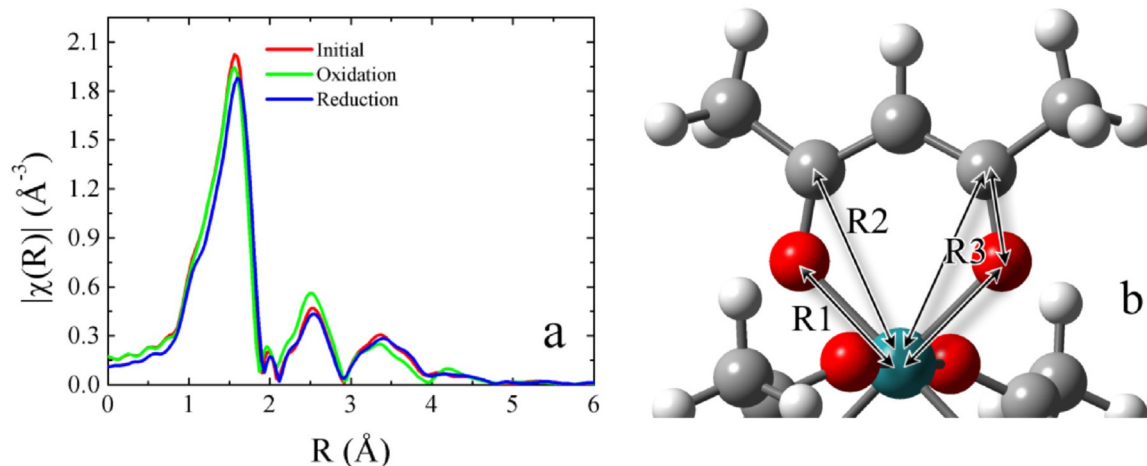
Figure 3. a) *R*-space EXAFS of Ru(acac)₃ before BE and following reduction and oxidation (*k*-weight = 2). Peaks at 1.6 and 2.5 are primarily formed from the illustrated photoelectric paths in (b). The peak at 3.3 Å consists of a large number of ligand paths which could not be deconvoluted.

Figure 4. Changes in Ru—O bond length (Ru—O first shell) for Ru(acac)₃ during BE, as determined by using in situ EXAFS.

and Ru(acac)₃⁻—the change in bond distances between them was too small to deconvolute into separate paths. Instead, the bond length was taken as an average for these species. Variations in the bond length determined by using EXAFS were consistent with those calculated by DFT (Table 2). The optimized structure, *XYZ* coordinates, and bond-length changes can be found in Figure S5 and Tables S1 and S2 in the Supporting Information. The acetylacetonate ligand is negatively charged and, as the complex is reduced, the Ru—O bond should lengthen, owing to repulsive forces; the opposite should occur with an increasing oxidation state. Interestingly,

variations in R2 and R3 path distances were less than the estimated uncertainties, indicating minor changes in the corresponding bond lengths, if any. The uncertainties for R2 and R3 are 0.02 and 0.05 Å, respectively, so the photoelectron path length is likely changing, but within error. Alternatively, the ligand is distorted to allow for a slight increase in R1, without changing R2 or R3. The full set of EXAFS data are provided in the Supporting Information (Table S3) along with a representative fit (Figure S6). Recall that there were minimal changes in the electrochemistry observed from cyclic voltammograms collected before and after BE to reduce Ru(acac)₃ (Figure 2). The reversible Ru—O bond changes are consistent with those findings.

When Ru(acac)₃ was electrochemically oxidized, the Ru—O bond length (Figure 4) decreased by less than 0.01 Å; the small change was linear with the charge extracted. As was found during the reduction of Ru(acac)₃, the amplitude of each EXAFS path does not deviate from 1.0 ± 0.1; ligand shedding, if any, was less than 10 %. This result is apparently inconsistent with the voltammograms, which indicated significant changes in the electrochemistry (Figure 2) and presumably the structure of Ru(acac)₃ upon oxidation. Based on the DFT calculations, a bond-length change of 0.04 Å should occur when Ru(acac)₃ is oxidized to [Ru(acac)₃]⁺, providing further evidence for a species other than [Ru(acac)₃]⁺. The EXAFS spectra allowed us to rule out the formation of RuO₂ (1.9 Å Ru—O bond), a Ru acetylacetonate dimer (2.6 Å Ru—Ru bond), or Ru metal (2.5 Å Ru—Ru bond) as products.[40] As our EXAFS measurements in the 3–6 Å range do not include enough data to deconvolute the large number of overlapping photoelectron paths generated by the acetylacetone ligand, we do not expect to observe any changes on the ligand 3 Å from the Ru atoms. We have tentatively concluded that the structural and compositional changes occurred on the acetylacetone ligand, beyond the sampling range of EXAFS. The changes were irreversible and the resulting complex produces a couple at −0.2 V versus Ag/Ag⁺. Ru XANES will provide important information regarding relative contributions of the Ru and the ligand to the electrochemistry.

Table 2. Measured (EXAFS) and computed (DFT) bond-length changes after reduction and oxidation of Ru(acac)₃.

Average Ru—O bond-length change	[Ru(acac)₃]⁻¹	[Ru(acac)₃]⁺¹
experimental [Å]	0.03 ± 0.01	−0.01 ± 0.01
computed [Å]	0.043	−0.042

Nevertheless, additional characterization will be required to provide a highly detailed description of the species.

2.3. Charge Distribution During Reduction and Oxidation

The ligands on metal acetylacetonates are typically considered to be redox innocent, that is, they do not contribute to the electrochemistry.[41] By tracking the oxidation state of Ru, we can determine the degree of innocence or non-innocence. One would expect the Ru oxidation states to change by ± 1 if only the metal participated. The change in the charge on Ru following BE of $Ru(acac)_3$ was quantified by tracking edge shifts in the in situ XANES spectra (see Figure 5). The Ru edge shifted to lower energy during reduction and to higher energy during oxidation, and these shifts were reversible. For both reactions, the post-edge features did not change significantly. A shift of $+1.25$ eV corresponds to a $+1$ change in the oxidation state of Ru (Figure 6a) based on the correlation of edge shifts for known standards (results for the standard samples can be found in Figure S7). Given this correlation, the oxidation state of Ru decreases from 2.2 ± 0.2 to 1.0 ± 0.2 during the reduction

of $Ru(acac)_3$ (Figure 6b). In other words, most of the electrochemistry is attributed to Ru. Also note that XANES spectra after reoxidizing the reduced $Ru(acac)_3$ (returning to zero electrons per molecule) were nearly identical to those for the fresh electrolyte.

Following electrochemical oxidation of $Ru(acac)_3$, the oxidation state of Ru increases from 2.2 ± 0.2 to 2.9 ± 0.2, or a net change of 0.7 ± 0.2. The results indicate that, although most of the electrochemistry can be attributed to the Ru, significant charge (ca. $30 \pm 20\%$) is extracted from other constituents of the complex, namely the ligands. Given differences in products for the reduction and oxidation reactions, one might conclude that the stability of $Ru(acac)_3$ is correlated with the degree of charge that is stored on or extracted from Ru.

Experimentally determined changes in the oxidation states were compared to the quantified HOMO and LUMO densities determined from the DFT calculations (Table 3). A complete list of the orbital densities for each atom at each charge state for $Ru(acac)_3$ can be found in the Supporting Information (Table S4). In all cases, DFT calculations indicate less of the orbital density to be on the metal than determined from the
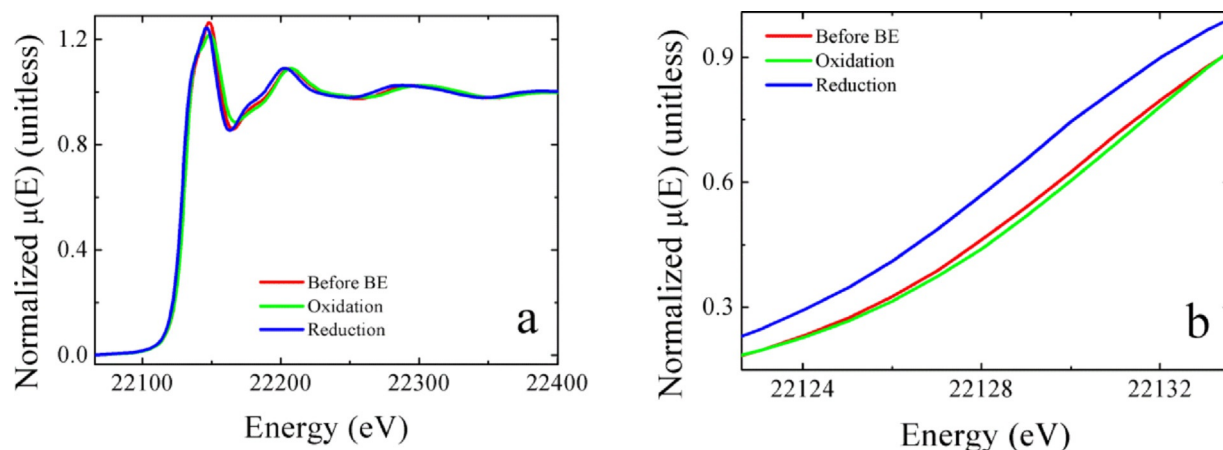

Figure 5. a) Full and b) edge XANES of $Ru(acac)_3$ solutions following reduction and oxidation through BE.
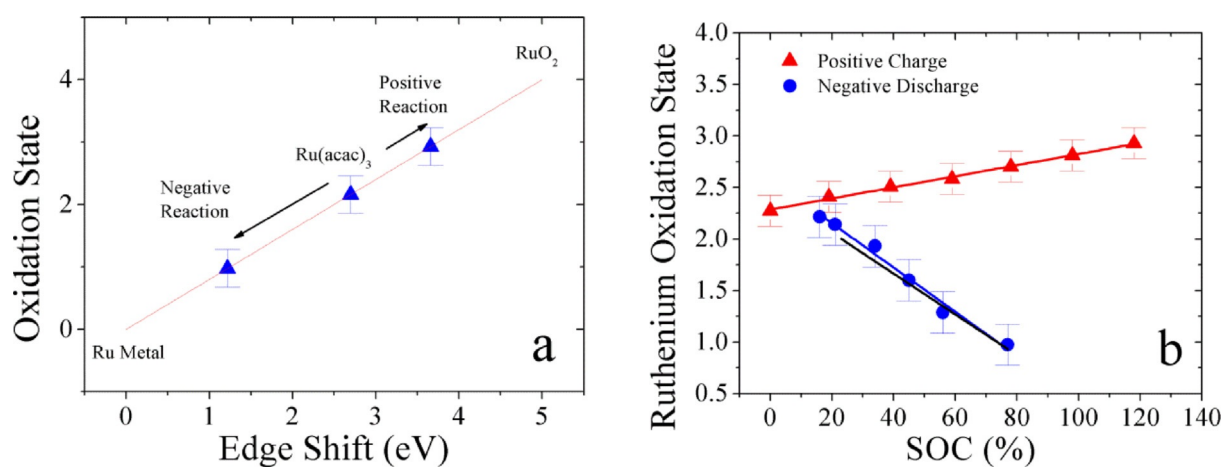

Figure 6. a) Edge shifts for standards and charged species associated with reduction and oxidation reactions (determined from standards) and b) XANES-estimated oxidation states of samples during reduction (black/blue) and oxidation (red).

Table 3. Changes of oxidation state for Ru in Ru(acac)$_3$ during oxidation and reduction determined from XANES. The results are compared to the fraction of the orbital density determined from DFT calculations.

Method	Reduction	Oxidation
XANES	-1.2 ± 0.2	0.7 ± 0.2
DFT	-0.67	0.53

XANES results; this is not unexpected, as DFT is known to distribute charge throughout a complex.[36] Regardless, DFT predicts more of the orbital density to be on Ru during reduction of Ru(acac)$_3$ than during oxidation, which is in agreement with the experimental results. The orbital densities for each atom type determined from the DFT calculations are shown in Figure 7. For the oxidized Ru(acac)$_3$ electrolyte, more of the orbital density is on the oxygen atoms than for the reduced Ru(acac)$_3$ electrolyte, and likewise for the carbon atoms, specifically those that are part of the conjugated ring portion of the acetylacetone ligands.
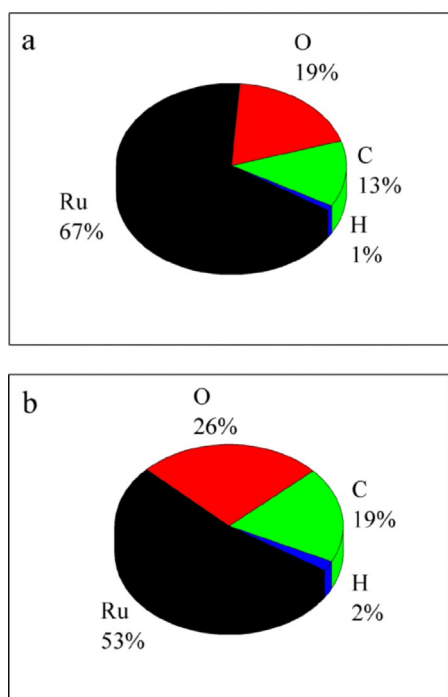
Figure 7. Neutral Ru(acac)$_3$ orbital density by atom type for a) LUMO and b) HOMO.

Both XANES and EXAFS of the oxidation reaction indicate that the side reaction likely occurred on the conjugated portion of the ligands. K-edge XANES typically generates a pre-edge peak, except when this is suppressed by inversion symmetry (e.g. octahedral) around the metal; this is a common method of quantifying transitions from octahedral (no pre-edge) to tetrahedral (strong pre-edge) environments in metals. In the case of Ru, a weak pre-edge shoulder is expected at 22 118 eV for non-inversion-symmetric species.[42] The lack of

this feature in oxidized Ru(acac)$_3$ (Figure 5) indicates octahedral symmetry is maintained. Insights derived from results presented in this paper are being used to functionalize the acetylacetone to mitigate side reactions.

3. Conclusions

The experimental and computational results presented in this paper indicate the reversible reduction of Ru(acac)$_3$ to [Ru(acac)$_3$]$^-$ in acetonitrile, with essentially all of the charge localized to the metal center and the Ru−O bond length increasing on reduction and contracting during reoxidation. The oxidation of Ru(acac)$_3$ in acetonitrile appeared to initially produce [Ru(acac)$_3$]$^+$, which converted to another species through chemical or electrochemical processes. Approximately 70 % of the charge was extracted from the Ru atom and approximately 30 % from the acetylacetone ligands. Collectively, the results suggest that, although the short-term product of Ru(acac)$_3$ oxidation could be [Ru(acac)$_3$]$^+$, the long-term product has six-fold Ru−O bonding with octahedral symmetry, has a structure that is identical to Ru(acac)$_3$ up to 3 Å from Ru, has a Ru oxidation state of 2.9 ± 0.2, and produced a couple at −0.2 V versus Ag/Ag$^+$, which was found to be irreversible during BE. The results also indicate that stability and cyclability are functions of the degree of charge transfer with the metal center. Additional research will determine if this behavior is common to other metal acetylacetonates as well as other complexes.

Experimental Section

Cyclic Voltammetry

CV was performed by using a PGSTAT302N Autolab potentiostat. A 10 mL, three-electrode electrochemical cell, fabricated in-house, was used for these experiments. The three electrodes consisted of a 0.07 cm^2 glassy carbon disk working electrode (BASi), a Ag/Ag$+$ quasi-reference electrode (BASi) filled with 0.01 M silver tetrafluoroborate in acetonitrile (Sigma Aldrich), and a 23 cm long platinum wire counter electrode (ALS). The working electrode was polished by using 9 and 0.3 µm aluminum oxide polishing paper (Fiber Instrument). Electrolyte solutions were prepared inside an Ar-filled VAC glove box, and all CV scans were conducted inside the same glove box.

Bulk Electrolysis

BE was performed by using a PGSTAT100 Autolab potentiostat with a chronoamperometric method. Holding potentials were chosen to isolate individual redox couples but avoid expected side reactions. A 10 mL, glass cell consisting of two equal volume working and counter chambers separated by a class P5 (1.0–1.6 µm pore size) glass frit (Adams&Chittenden) was fabricated in-house. The working electrodes were made from reticulated vitreous carbon sheets with 60 pores per inch (ERG Aerospace) that were cut into rectangular strips (ca. $1 \times 1 \times 5$ cm^3). 0.07 cm^2 glassy carbon working electrodes were used for in situ CV measurements, which were polished by using 9 and 0.3 µm aluminum oxide polishing paper (Fiber Instrument). A Ag/Ag$^+$ quasi-reference electrode (BASi) filled with 0.01 M silver tetrafluoroborate in acetonitrile (Sigma Aldrich) was used as the reference electrode, and a 23 cm

long platinum wire (ALS) was used as the counter electrode. Two Teflon stirrer bars were used to mix the counter and working solutions during the experiments, and stirring was temporarily stopped during CV measurements. For Ru(acac)$_3$, constant voltage BE was performed at a concentration of 0.1 M active species with 0.5 M TBABF$_4$ in acetonitrile. The same electrolyte was used in the counter chamber (equal volume as the working chamber). To characterize the oxidation reaction, the materials were evaluated following BE at 0.8 and 0.4 V versus Ag/Ag$^+$. To characterize the reduction reaction, the materials were evaluated following BE at −1.5 and −0.7 V versus Ag/Ag$^+$. A current cut-off of 1 mA was used for both reactions as cross-over occurs in the cell and a current lower than 1 mA would not be reached. Samples before and after BE were diluted to 0.01 M active species with 0.1 M TBABF$_4$ in acetonitrile and cyclic voltammgrams were collected.

X-ray Absorption Spectroscopy

XAS experiments were performed at beamline 10-BM (MRCAT) of the Advanced Photon Source, Argonne National Laboratory. Beam size was set at 0.5×0.5 mm and experiments were conducted in transmission mode with gas ionization chambers. XANES analysis consisted of observing changes in edge shift as well as transitions from one species to another, as calculated through linear combination fitting (LCF) to known standards.

X-ray collection was taken from 200 eV below the K edge of Ru metal (Ru K $E_0 = 22\,117$ eV) to approximately 1200 eV above the edge (ca. 18 Å^{-1}) with each measurement taken over the course of 30 min. EXAFS analysis was completed by using the AUTOBK algorithm with a spline range of 0–18 Å^{-1}, Rbkg = 1.0, and a normalization order of 3. The EXAFS range was found to be excellent to 18 Å^{-1} and a Fourier transform was made by using $3 < k < 16$ A^{-1}.

Measurement of Ru standards of Ru metal, Ru(acac)$_3$, tris(triphenylphosphine) ruthenium (II) dichloride (TTP-RuCl$_2$), RuO$_2$, and RuCl$_3$ were taken in polycarbonate cuvettes (liquid samples) or ground to a fine powder and loaded into polyimide tape packets (solid samples).

A BE cell was placed in the beamline such that a 1 cm length of electrolyte could be measured in transmission mode (edge step ca. 0.7). The negative and positive reactions were tested separately by conducting BE of the individual half-reactions charged from 0% ("before electrolysis") to the maximum electrons per molecule in steps of 0.2, and subsequent discharge, with XAS measurement taken at each step. The BE experiment was conducted by using the same method as described above when using the Teflon cell. For the reduction reaction, the electrons per molecule were determined by using the open-circuit potential and the Nernst equation. For the oxidation reaction, the open-circuit potential was not a reliable method of determining the electrons per molecule, owing to the side reaction changing the open-circuit potential. Monitoring of current during each step demonstrated negligible changes in the oxidation state of the electrolyte while XAS was being collected.

Density Function Theory Calculations

Structure optimization calculations were performed for the neutral and charged species by using the B3LYP functional with the 6–31+G(d) and LANL2DZ basis sets. All minimized structures were confirmed through vibrational frequency calculations. The B3LYP functional with the 6–31+G(d) basis set has previously been

shown to be effective at determining the standard potentials of both ionic liquids and quinoxaline derived complexes,[43,44] and similar DFT calculations have been shown to correctly predict the reduction standard potentials of various metal–acetylacetonate complexes. In previous metal–acetylacetonate studies, no oxidation potentials, structural changes during charge/discharge, or charge states were presented.[45] The LANL2DZ basis set has been used for complexes similar to Ru(acac)$_3$ to effectively determine the charge of the metal versus the ligand for neutral species by using natural population analysis (NPA), and calculating molecular orbital energies.[46] First, the predicted standard potentials were calculated by using the highest occupied molecular orbitals (HOMO) and lowest unoccupied molecular orbitals (LUMO) values of the neutral species in acetonitrile by using the polarizable continuum model (PCM). A linear correlation found by Cheng et al. for 295 organic complexes[43] was used to convert the calculated HOMO and LUMO energies to the positive and negative standard potentials, respectively. The optimized structures with different charges were compared to determine any significant changes in bond lengths and angles to compare with the XAS results.

To quantify the HOMO and LUMO density for the complex, Multiwfn, a multifunctional wavefunction analyzer developed by Beijing Kein Research Center for Natural Sciences was utilized, using the Hirshfeld method.[37]

Cell Design

A custom Teflon cell was built for use in the in situ XAS experiments run at Argonne National Lab, constructed in the Physics machine shop at the University of Michigan. The cell consisted of three parts: a working electrode chamber, a counter electrode chamber, and a block used to seal a P5 glass frit (Adams & Chittenden) between the two electrode chambers. The dimensions of the counter and working electrode cavities were designed to ensure that the liquid heights were equal when using 5 mL of solution in both chambers. The counter electrode chamber (shown on the left side of all explosion diagrams in Figure 8 consists of a 2″ cavity of 0.625″ diameter. At the top of the cavity was threading for a 1/2″ NPT fitting, where a Pt wire counter electrode was secured using a $\frac{1}{4}$″ Swagelok ultra-Torr fitting. A 0.9 cm diameter hole was cut into the cavity with an expanded diameter (to 1 cm diameter) at the edge to house a #12 viton O-ring. In the middle connecting block, a 1 cm diameter hole was cut 8 mm into the 1 cm slab, with the last 2 mm consisting of a reduced hole of 0.9 cm diameter to house a #12 viton O-ring. The working electrode chamber
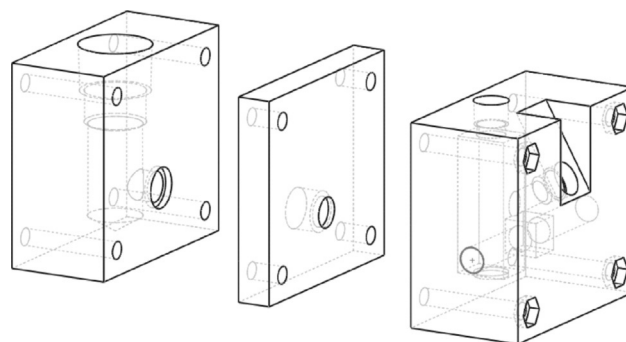
Figure 8. Explosion diagrams of the bulk electrolysis cell used in the in situ X-ray absorption experiments. From left to right: counter electrode block, connected block, working electrode block.

(Figure 9) consisted of a large rectangular cavity to house the working and reference electrodes, and a 1 cm×1 cm×1 cm cavity, which acted as the viewing area for X-rays. 7.5 mm diameter holes were cut into the sides of the $1\times1\times1$ cm^3 cavity, leaving Teflon walls that were approximately 250 μm thick, which acted as "win-
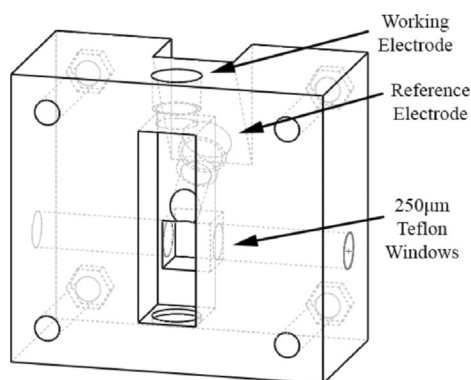

Figure 9. Schematic of working electrode chamber.

dows" for the X-rays while maintaining an air-tight seal. The working electrode chamber was sealed against the connecting block by using a #26 Viton O-ring, housed in an O-ring cutout. The working electrode, a $1\times1\times5$ cm^3 strip of 60 pore per inch reticulated vitreous carbon (ERG Aerospace) attached to a wire by using silver epoxy and a 7 mm glass tube, was secured at the top of the working electrode chamber by using a 1/4" Swagelok ultra-Torr fitting with an 1/8" NPT outlet. The reference electrode (Ag/Ag$^+$) was similarly secured by using a 1/4" ultra-Torr to 1/8" NPT Swagelok fitting at a 30° angle to the bottom face, aimed at contacting the top of the liquid in the cell. Prior to the experiments at Argonne National Lab, the cell was validated at UM by performing BE on a 0.1 M Ru(acac)$_3$ with 0.5 M TBABF$_4$ in acetonitrile solution, with similar results obtained in the glass BE cell (Figure 10). Furthermore, cyclic voltammograms were obtained to ensure no peaks associated with water or unknown products were found following air
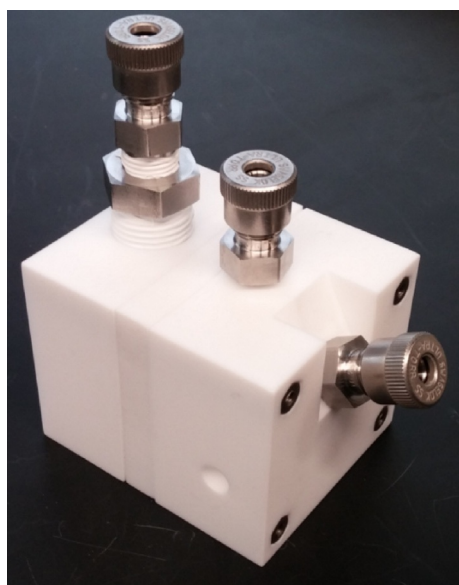

Figure 10. Assembled BE cell.

exposure to the Teflon cell for 12 h, which is well in excess of the time required for the BE experiments.

[1] A. Z. Weber, M. M. Mench, J. P. Meyers, P. N. Ross, J. T. Gostick, Q. Liu, *J. Appl. Electrochem.* **2011**, *41*, 1137.
[2] P. Denholm, E. Ela, B. Kirby, M. Milligan, *Contract* **2010**, *NREL*, 1.
[3] L. Jörrissen, H. Frey, *Encycl. Electrochem. Power Sources* **2009**, 215.
[4] U. S. Department of Energy, Grid Energy Storage, **2013**, 33.
[5] W. Wang, Q. Luo, B. Li, X. Wei, L. Li, Z. Yang, *Adv. Funct. Mater.* **2013**, *23*, 970.
[6] A. J. Bard, L. R. Faulkner, *Electrochemical Methods: Fundamentals and Applications*, John Wiley & Sons, Inc., New York, NY, **2001**.
[7] R. M. Darling, K. G. Gallagher, F. R. Brushett, *Energy Environ. Sci.* **2014**, *7*, 3459.
[8] P. J. Cappillino, H. D. Pratt, N. S. Hudak, N. C. Tomson, T. M. Anderson, M. R. Anstey, *Adv. Energy Mater.* **2014**, *4*, 1300566.
[9] Y. Huang, S. Gu, Y. Yan, S. F. Y. Li, *Curr. Opin. Chem. Eng.* **2015**, *8*, 105.
[10] P. J. Cabrera, X. Yang, J. A. Suttil, K. L. Hawthorne, R. E. M. Brooner, M. S. Sanford, L. T. Thompson, *J. Phys. Chem. C* **2015**, *119*, 15882.
[11] S.-H. Shin, S.-H. Yun, S.-H. Moon, *RSC Adv.* **2013**, *3*, 9095.
[12] D. Zhang, H. Lan, Y. Li, *J. Power Sources* **2012**, *217*, 199.
[13] H. D. Pratt, N. S. Hudak, X. Fang, T. M. Anderson, *J. Power Sources* **2013**, *236*, 259.
[14] Y. Matsuda, K. Tanaka, M. Okada, Y. Takasu, M. Morita, T. Matsumura-Inoue, *J. Appl. Electrochem.* **1988**, *18*, 909.
[15] T. Yamamura, Y. Shiokawa, H. Yamana, H. Moriyama, *Electrochim. Acta* **2002**, *48*, 43.
[16] L. Cosimbescu, X. Wei, M. Vijayakumar, W. Xu, M. L. Helm, S. D. Burton, C. M. Sorensen, J. Liu, V. Sprenkle, W. Wang, *Sci. Rep.* **2015**, *5*, 14117.
[17] I. L. Escalante-Garcia, J. S. Wainright, L. T. Thompson, R. F. Savinell, *J. Electrochem. Soc.* **2014**, *162*, A363.
[18] T. Herr, P. Fischer, J. Tübke, K. Pinkwart, P. Elsner, *J. Power Sources* **2014**, *265*, 317.
[19] T. Herr, J. Noack, P. Fischer, J. Tübke, *Electrochim. Acta* **2013**, *113*, 127.
[20] A. E. S. Sleightholme, A. A. Shinkle, Q. Liu, Y. Li, C. W. Monroe, L. T. Thompson, *J. Power Sources* **2011**, *196*, 5742.
[21] A. A. Shinkle, A. E. S. Sleightholme, L. D. Griffith, L. T. Thompson, C. W. Monroe, *J. Power Sources* **2012**, *206*, 490.
[22] Q. Liu, A. A. Shinkle, Y. Li, C. W. Monroe, L. T. Thompson, A. E. S. Sleightholme, *Electrochem. Commun.* **2010**, *12*, 1634.
[23] A. A. Shinkle, A. E. S. Sleightholme, L. T. Thompson, C. W. Monroe, *J. Appl. Electrochem.* **2011**, *41*, 1191.
[24] Q. Liu, A. E. S. Sleightholme, A. A. Shinkle, Y. Li, L. T. Thompson, *Electrochem. commun.* **2009**, *11*, 2312.

[25] A. A. Shinkle, T. J. Pomaville, A. E. S. Sleightholme, L. T. Thompson, C. W. Monroe, *J. Power Sources* **2014**, *248*, 1299.

[26] J. A. Suttil, J. F. Kucharyson, I. L. Escalante-Garcia, P. J. Cabrera, B. R. James, P. R. F. Savinell, M. S. Sanford, L. Thompson, *J. Mater. Chem. A* **2015**, *3*, 7929.

[27] M. H. Chakrabarti, R. A. W. Dryfe, E. P. L. Roberts, *Electrochim. Acta* **2007**, *52*, 2189.

[28] J. Mun, M.-J. Lee, J.-W. Park, D.-J. Oh, D.-Y. Lee, S.-G. Doo, *Electrochem. Solid-State Lett.* **2012**, *15*, A80.

[29] W. Wang, W. Xu, L. Cosimbescu, D. Choi, L. Li, Z. Yang, *Chem. Commun.* **2012**, *48*, 6669.

[30] X. Wei, W. Xu, M. Vijayakumar, L. Cosimbescu, T. Liu, V. Sprenkle, W. Wang, *Adv. Mater.* **2014**, *26*, 7649.

[31] B. Huskinson, M. P. Marshak, C. Suh, S. Er, M. R. Gerhardt, C. J. Galvin, X. Chen, A. Aspuru-Guzik, R. G. Gordon, M. J. Aziz, *Nature* **2014**, *505*, 195.

[32] J. Huang, L. Su, J. a. Kowalski, J. L. Barton, M. Ferrandon, A. K. Burrell, F. R. Brushett, L. Zhang, *J. Mater. Chem. A* **2015**, *3*, 14971.

[33] G. Nagarjuna, J. Hui, K. J. Cheng, T. Lichtenstein, M. Shen, J. S. Moore, J. Rodriguez-Lopez, *J. Am. Chem. Soc.* **2014**, *136*, 16309.

[34] X. Wei, L. Cosimbescu, W. Xu, J. Z. Hu, M. Vijayakumar, J. Feng, M. Y. Hu, X. Deng, J. Xiao, J. Liu, V. Sprenkle, W. Wang, *Adv. Energy Mater.* **2015**, *5*, 1400678.

[35] C. a. Apblett, D. M. Stewart, R. T. Fryer, J. C. Sell, H. D. I. Pratt, T. M. Anderson, R. W. Meulenberg, *Electrochim. Acta* **2015**, *185*, 156.

[36] Gaussian 09, Revision E.01, M. J. Frisch, G. W. Trucks, H. B. Schlegel, G. E. Scuseria, M. A. Robb, J. R. Cheeseman, G. Scalmani, V. Barone, B. Mennucci, G. A. Petersson, H. Nakatsuji, M. Caricato, X. Li, H. P. Hratchian, A. F. Izmaylov, J. Bloino, G. Zheng, J. L. Sonnenberg, M. Hada, M. Ehara, K. Toyota, R. Fukuda, J. Hasegawa, M. Ishida, T. Nakajima, Y. Honda, O. Kitao, H. Nakai, T. Vreven, J. Montgomery, J. A., J. E. Peralta, F. Ogliaro, M. Bearpark, J. J. Heyd, E. Brothers, K. N. Kudin, V. N. Staroverov, R. Kobayashi, J. Normand, K. Raghavachari, A. Rendell, J. C. Burant, S. S. Iyengar, J. Tomasi, M. Cossi, N. Rega, J. M. Millam, M. Klene, J. E. Knox, J. B. Cross, V. Bakken, C. Adamo, J. Jaramillo, R. Gomperts, R. E. Stratmann, O. Yazyev, A. J. Austin, R. Cammi, C. Pomelli, J. W. Ochterski, R. L. Martin, K. Morokuma, V. G. Zakrzewski, G. A. Voth, P. Salvador, J. J. Dannenberg, S. Dapprich, A. D. Daniels, Ö. Farkas, J. B. Foresman, J. V. Ortiz, J. Cioslowski, D. J. Fox, **2009**.

[37] N. M. O'Boyle, A. L. Tenderholt, K. M. Langner, *J. Comput. Chem.* **2008**, *29*, 839.

[38] M. A. Nawi, T. L. Riechel, *Inorg. Chem.* **1981**, *20*, 1974.

[39] H. Ikeuchi, K. Naganuma, M. Ichikawa, H. Ozawa, T. Ino, M. Sato, H. Yonezawa, S. Mukaida, A. Yamamoto, T. Hashimoto, *J. Solution Chem.* **2007**, *36*, 1243.

[40] S. Kar, N. Chanda, S. M. Mobin, A. Datta, F. A. Urbanos, V. G. Puranik, R. Jimenez-aparicio, G. K. Lahiri, *Inorg. Chem.* **2004**, *43*, 4911.

[41] Z. Zhang, S. S. Zhang, *Rechargeable Batteries: Materials, Technologies and New Trends*, Springer International Publishing, Switzerland, **2015**.

[42] K. Getty, M. U. Delgado-Jaime, P. Kennepohl, *Inorg. Chim. Acta* **2008**, *361*, 1059.

[43] L. Cheng, R. S. Assary, X. Qu, A. Jain, S. P. Ong, N. N. Rajput, K. Persson, L. A. Curtiss, *J. Phys. Chem. Lett.* **2015**, *6*, 283.

[44] N. Shao, X. Sun, S. Dai, D. Jiang, *J. Phys. Chem. B* **2011**, *115*, 12120.

[45] R. Freitag, Computational, Structural and Electrochemical Properties of Metal(III)tris-betadiketonato Complexes, University of the Free State, Dissertation, **2013**.

[46] D. Kalinina, C. Dares, H. Kaluarachchi, P. G. Potvin, A. B. P. Lever, *Inorg. Chem.* **2008**, *47*, 10110.